Self healing of radiation-induced damage in Fe–Au and Fe–Cu alloys

Combining positron annihilation spectroscopy with TEM and ab initio calculations

Zhang, Shasha; Cizek, Jakub; Yao, Zhengjun; Oleksandr, Moliar; Kong, Xiangshan; Liu, Changsong; van Dijk, Niels; van der Zwaag, Sybrand

DOI
10.1016/j.jallcom.2019.152765

Publication date
2020

Document Version
Final published version

Published in
Journal of Alloys and Compounds

Citation (APA)
Zhang, S., Cizek, J., Yao, Z., Oleksandr, M., Kong, X., Liu, C., van Dijk, N., & van der Zwaag, S. (2020). Self healing of radiation-induced damage in Fe–Au and Fe–Cu alloys: Combining positron annihilation spectroscopy with TEM and ab initio calculations. *Journal of Alloys and Compounds*, *817*, Article 152765. https://doi.org/10.1016/j.jallcom.2019.152765

Journal of Alloys and Compounds 817 (2020) 152765

Contents lists available at ScienceDirect

Journal of Alloys and Compounds

journal homepage: http://www.elsevier.com/locate/jalcom

Self healing of radiation-induced damage in Fe–Au and Fe–Cu alloys: Combining positron annihilation spectroscopy with TEM and *ab initio* calculations

Shasha Zhang [a, c, *], Jakub Cizek [b], Zhengjun Yao [a, c], Moliar Oleksandr [a, c], Xiangshan Kong [d, **], Changsong Liu [d], Niels van Dijk [e], Sybrand van der Zwaag [f, g]

[a] College of Materials and Technology, Nanjing University of Aeronautics and Astronautics, Nanjing, 211106, People's Republic of China
[b] Department of Low Temperature Physics, Faculty of Mathematics and Physics, Charles University, Prague, 8 CZ-18000, Czech Republic
[c] Key Laboratory of Materials Preparation and Protection for Harsh Environment (Nanjing University of Aeronautics and Astronautics), Ministry of Industry and Information Technology, Nanjing, 211106, People's Republic of China
[d] Key Laboratory of Materials Physics, Institute of Solid State Physics, Chinese Academy of Sciences, P.O. Box 1129, Hefei, 230031, People's Republic of China
[e] Fundamental Aspects of Materials and Energy group, Faculty of Applied Sciences, Delft University of Technology, Mekelweg 15, 2629 JB, Delft, the Netherlands
[f] Novel Aerospace Materials group, Faculty of Aerospace Engineering, Delft University of Technology, Kluyverweg 1, 2629 HS, Delft, the Netherlands
[g] School of Materials Science and Engineering, Tsinghua University, Beijing, People's Republic of China

ARTICLE INFO

Article history:
Received 26 July 2019
Received in revised form
11 October 2019
Accepted 21 October 2019
Available online 23 October 2019

Keywords:
Self-healing
Au/Cu precipitation
Radiation-induced defects
Positron annihilation spectroscopy
Ab initio calculations
bcc Fe

ABSTRACT

Self healing of early stage radiation damage by site selective solute segregation is a promising approach to extend the lifetime of nuclear reactor components. In the present study, the creation and autonomous healing of irradiation-induced damage is investigated in pure Fe and high purity Fe–Au and Fe–Cu model alloys. To create radiation damage samples are irradiated at 550 °C by 120 keV He^+ ions with fluences of 5.0×10^{15}, 1.0×10^{16} and 5.0×10^{16} ions/cm^2. The observed increase in the *S* and *W* parameters determined in the variable energy positron annihilation spectroscopy measurements indicates the formation of vacancy-like defects, precipitates and vacancy-solute complexes. The presence of substitutionally dissolved Au is found to reduce the formation of radiation defects more efficiently than solute Cu. Site-specific Au precipitation at defect sites is indicated, which results in damage healing with a reduced swelling, whereas Cu precipitates and radiation damage only show weak interaction. *Ab initio* calculations show that the binding energies of Au solutes to vacancy clusters ($Au\text{-}V_n$) are significantly larger than those of Cu solutes ($Cu\text{-}V_n$) whereas the binding energies of helium filled vacancy clusters $Au\text{-}He_nV_n$ and $Cu\text{-}He_nV_n$ are comparable.

1. Introduction

The irradiation of steel components close to the core of a nuclear reactor by neutrons, ions and electrons unavoidably leads to microstructural damage, in the form of vacancies, dislocations, voids and He bubbles [1]. These types of damage ultimately lead to swelling, hardening, amorphization and embrittlement, limiting the lifetime and stability of critical structural components of nuclear reactors [2,3]. Self-healing of irradiation-induced damage is thought to be a promising approach to enhance the resistance against irradiation and thereby extend the lifetime of the materials used in nuclear reactors, including the reactor vessel itself [4]. Self-healing has recently been put forward as a promising new mechanism to mitigate microscopic or even mesoscopic mechanical damage, in the form of cracks and scratches, and to enhance the component lifetime for polymers [5,6], ceramics [7,8] and concrete [9]. In comparison to these materials the development of self-healing metals remains challenging due to the small size of the metal atoms, their low atomic mobility at non-elevated temperatures and the fact that the metallic bond is directionally isotropic [10,11].

* Corresponding author. College of Materials and Technology, Nanjing University of Aeronautics and Astronautics, Nanjing, 211106, People's Republic of China
** Corresponding author. Key Laboratory of Materials Physics, Institute of Solid State Physics, Chinese Academy of Sciences, P.O. Box 1129, Hefei, 230031, People's Republic of China.
E-mail addresses: s.zhang@nuaa.edu.cn (S. Zhang), xskong@issp.ac.cn (X. Kong).

https://doi.org/10.1016/j.jallcom.2019.152765
0925-8388/

Bai and coworkers [12] were the first to present a self-healing mechanism for radiation damage in copper using atomistic simulation methods. The calculated results showed that under typical reactor irradiation conditions grain boundaries can act as sinks and absorb interstitials, while emitting interstitials to recombine with vacancies. Some years later, a similar self-healing mechanism was reported for iron [13]. Recently the addition of oversized W in Fe was found to suppress the formation of large defect clusters using molecular dynamics simulations [14]. Borovikov et al. [15] proposed a radiation-damage healing mechanism in tungsten by the induced motion of grain boundaries. The above studies yielded some insight into the self-healing mechanism of radiation damage in metals and provided some qualitative guidelines on how to make use of the self-healing concept in pure metals and metal alloys. However, so far only a few experimental studies on the self-healing of radiation damage in metals have been reported. Recently, the self-healing of twin boundaries was observed by an in situ study of the defect migration kinetics in heavy ion irradiated Ag [16].

Besides the intrinsic self healing of defects in metals near grain boundaries and twin boundaries, the site-specific segregation and subsequent precipitation of dissolved alloying atoms has a high potential to achieve self-healing of irradiation induced damage. Based on the Johnson-Lam model, the segregation and precipitation of substitutionally dissolved solute atoms is predicted to occur in non-precipitated alloys under irradiation conditions [17]. When the solute atoms are strongly attracted to the irradiation-induced defects, they will segregate and precipitate on the damage sites, realizing self-healing by a reduction in swelling (and by immobilizing the growth of the defect structures). The radiation-induced solute redistribution can result in a reduction of the swelling [18,19].

Cu, either present as an alloying element or as an impurity, is a commonly encountered element in steels used in nuclear reactors. Hence, the interaction between solute Cu atoms with radiation defects has been studied extensively. Molecular dynamic simulations revealed that Cu atoms in iron can act as sinks for both vacancies and interstitial defects and act as strong recombination centres under irradiation conditions [20,21]. Employing *ab initio* calculations, the interaction of Cu with irradiation defects, i.e., vacancies and helium atoms, was investigated and stable configurations of Cu-vacancy (Cu_nV_m) and Cu–He (Cu_nHe_m) complexes were indicated [22,23]. Experimentally, irradiation-induced Cu-rich aggregations were found in Fe–Cu model alloys and Cu-containing reactor pressure vessel steels [24,25]. Jin and coworkers revealed a spatial correlation between Cu precipitates and irradiation defects in Fe–Cu model alloys and using positron annihilation spectroscopy demonstrated the formation of Cu_nV_m complexes and cavities surrounded by tiny Cu precipitates [26,27]. Xu and coworkers reported the formation of Cu precipitates within newly formed micro-voids in neutron irradiated Fe–Cu model alloys [28,29]. This internal precipitation resulted in a shrinkage of the micro-voids. Notwithstanding all these results, limited coupled experimental and computational information is available on the role of Cu solutes and clusters thereof in improving the radiation swelling resistance of iron-based alloys and steels via self-healing of irradiation defects.

Although the relation between Cu precipitates and open volume defects has been widely studied in literature, the potential for solute Cu atoms to act as a self-healing agent in Fe-based alloys is limited, due to the fact that Cu is not only involved in the formation of precipitates surrounding the radiation defects, but also in the formation of Cu-rich precipitates in the undamaged matrix [30].

Recently, Au has been identified as an interesting high potential self-healing alloying element because of its following characteristics: (i) like Cu mobile solute Au can be dissolved in the ferritic iron matrix by an appropriate heat treatment; (ii) the energy barrier for homogeneous nucleation of Au precipitates in the Fe matrix is high due to the large size difference between solute and solvent atoms [31]; (iii) *ab-initio* calculations have predicted a strong interaction between solute Au and the irradiation-induced defects, in particular to vacancies and helium [32,33].

In the present study, the interaction between dissolved Au and Cu atoms and irradiation defects is studied in Fe–Au and Fe–Cu binary alloys of similar atomic solute concentration using variable energy positron annihilation spectroscopy (VEPAS) and transmission electron microscopy (TEM). The observed behaviour is analysed on the basis of complementary *ab-initio* calculations of the binding energy between either Cu or Au atoms and vacancies and clusters thereof.

2. Experimental and calculation methods

In order to clarify the role of alloying elements in the self-healing mechanism in real engineering steels, less complex low-alloyed model alloys are preferred in order to limited the number of potential reactions and interactions that can take place simultaneously. We therefore prepared via vacuum melting two high purity binary Fe–Au and Fe–Cu model alloys (both with ~1 at. % of solute atoms). For comparison, high-purity Fe samples were also prepared. The composition of the samples is listed in Table 1. The pure Fe sample was fully annealed at 850 °C for 1 h after casting and rolling whereas Fe–Au and Fe–Cu alloys were solution treated at 868 °C for 5 h and 850 °C for 1 h. All heat treatments were done in evacuated and sealed silica tubes filled with ultrahigh-purity argon gas and quenched into water at room temperature at the end of the heat treatment.

The specimens were irradiated using an ion implanter in the accelerator laboratory of Wuhan University. Irradiations were performed at 550 °C using 120 keV He^+ ions to fluences of 5×10^{15}, 1×10^{16} and 5×10^{16} ions/cm^2, corresponding to irradiation time of 0.8, 1.6 and 8 h, respectively. Variable energy positron annihilation spectroscopy (VEPAS) measurements were carried out on a magnetically guided slow positron beam with a ^{22}Na radiation source (activity of 1.85 GBq) and a W foil moderator. The energy of the positrons in the beam was varied from 0.08 to 35 keV. The relation between the energy of the incident positrons E and the mean positron penetration depth $\overline{Z}$ was calculated as follows [34]: $\overline{Z} = 40E^{1.6}/\rho$, where $\overline{Z}$ is expressed in nanometers, E is the incident positron energy in keV and ρ is the material density in g/cm^3. Doppler Broadening (DB) of the annihilation photon peak was measured using a high-purity Ge detector with the energy resolution of 1.1 keV at 511 keV. Two parameters (S and W) were calculated from the annihilation photo-peak. The S and W parameters were defined as the ratio of the number of counts in the central energy region (511 ± 0.75 keV) and in two high momentum regions (515.0–519.2 keV and 502.8–507.0 keV) of the annihilation photon peak normalized to the total number of counts in the overall peak, respectively. The energy range 511 ± 0.75 keV for calculation of the S parameter was chosen so that the bulk S parameter value for virgin Fe is close to 0.5 in order to guarantee that S parameter has the highest sensitivity for changes in the width of annihilation

Table 1
Chemical composition of the pure Fe samples and the Fe–Au and Fe–Cu alloy samples (in wt.% with balance iron).

Alloy	Au	Cu	C	P	S	Si
Fe	–	–	0.0014	0.0002	0.0001	0.0014
Fe–Au	4.20	–	0.0022	0.0206	0.0010	0.0255
Fe–Cu	–	1.15	0.0073	0.0054	<0.0010	0.0291

photo-peak. The central region for the *S* parameter was kept the same for all samples. The microstructures after irradiation were examined by TEM using a Tecnai F20ST/STEM instrument operating at 200 keV.

The *ab-initio* calculations were performed using the Vienna Ab-initio Simulation Package (VASP) based on the density functional theory [35]. The interactions between ions and electrons were described by the projector augmented wave potential (PAW) method [36]. The exchange-correlation energy functionals were described with the generalized gradient approximation as parameterized by Perdew-Burke-Ernzerhof [37]. Spin polarized calculations were conducted to account for the magnetic nature of Fe. A supercell composed of 128 lattice points, based on a $4 \times 4 \times 4$ bcc lattice, was used. A plane wave cutoff energy of 500 eV and a *k*-point density of $3 \times 3 \times 3$ was employed, which achieves a convergence of the total energy of the system to within 1 meV/atom. During the structural optimization, the shape and size of the supercell and atomic position were fully relaxed until the forces on all atoms are less than 0.01 eV/Å. The lattice constant of *bcc* Fe was calculated to be 2.83 Å, which agrees well with the experimental values [38] and previous DFT calculations [39].

The monovacancy formation energy was calculated using

$$E_f^V = E_{total}^V - \frac{127}{128} E_{total}^{Perfect} \quad (1)$$

where E_{total}^V and $E_{total}^{Perfect}$ are the total energies of the supercell with and without a vacancy, respectively.

The binding energies between two defects (such as A_1, A_2) was defined as follows:

$$E_b^{A_1-A_2} = E_{total}^{A_1} + E_{total}^{A_2} - E_{total}^{A_1-A_1} - E_{total}^{Perfect} \quad (2)$$

where $E_{total}^{A_1}$ and $E_{total}^{A_2}$ are the total energies of the supercell with A_1 and A_2, respectively, and $E_{total}^{A_1-A_1}$ is the total energy of the supercell containing both A_1 and A_2. Positive binding energies are attractive, while negative values are repulsive.

3. Results and discussion

3.1. Calculated He implantation and dpa profiles

For the used implantation energies the displacement per atom (dpa) and He concentration profiles as a function of depth are calculated using the Stopping and Range of Ions in Matter (SRIM) computer program [40]. The displacement energy of Fe was set to be 40 eV [41] and the calculation was based on the Kinchin-Pease mode, as recommended by Stoller et al. [42]. As shown in Fig. 1, for a fluence of 1.0×10^{16} ions/cm^2 the irradiation-induced damage reached a maximum value of approximately 0.25 dpa at the depth of 350 nm. The implanted He ions extended from the surface to a depth of about 600 nm and the maximum He concentration was approximately 0.6 at. % at a depth of 390 nm.

3.2. Variable energy positron annihilation spectroscopy

The evolution of the *S* and *W* parameters with increasing incident positron energy is shown in Fig. 2 for pure Fe, the Fe–Au and the Fe–Cu alloys irradiated with different fluences, together with data for the samples prior to irradiation. The *S* parameter represents the fraction of positron annihilations as a result of interactions with low momentum electrons and increases for an increasing volume fraction of vacancy-like defects. The *W* parameter reflects the fraction of positron annihilation with high momentum electrons. Since the positron affinity of Au and Cu is by

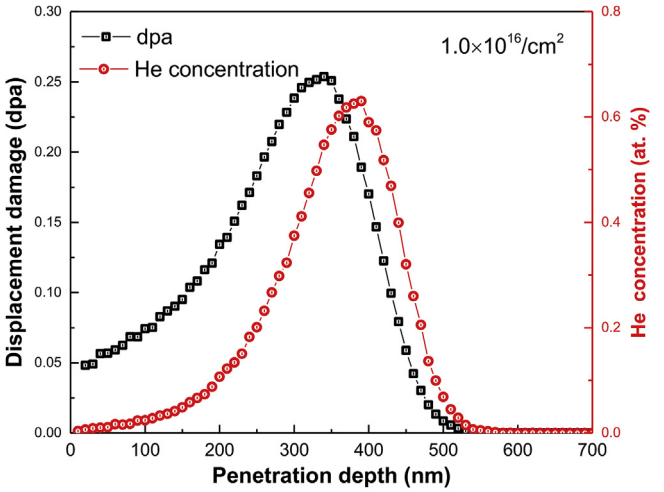

Fig. 1. Radiation damage in pure Fe for a fluence of 1.0×10^{16} ions/cm^2 in units of displacement per atom (dpa) and the corresponding helium concentration depth profile obtained from SRIM calculations.

0.75 and 0.97 eV lower than that of Fe [43], respectively, Au-rich and Cu-rich clusters (precipitates or solute-vacancy complexes) are regarded as preferential potential wells for the positrons. The annihilation of positrons with the Au-rich and Cu-rich clusters will cause an increase in the selected high momentum regions, resulting in high *W* parameters [30,44]. For all three materials the *S* parameters (Fig. 2(a)-2(c)) for irradiated samples are obviously enhanced compared to the unirradiated sample in the positron energy range from 5 to 20 keV. This enhancement becomes more pronounced for an increasing irradiation dose. The increase in *S* parameter is comparable for all three samples, but strongest for the pure Fe sample and weakest for the Fe–Au alloy sample.

The *W* parameters for the pure Fe samples (Fig. 2(d)) demonstrate a modest decrease for the irradiated samples. In contrast, an obvious increase in *W* parameter is observed for the irradiated Fe–Au and Fe–Cu alloys (Fig. 2(e) and (f)). This enhancement is ascribed to positron-detected Au/Cu-rich chemical environment representative for precipitates or solute-vacancy complexes. Besides the irradiation-induced precipitation, the Au and Cu precipitates will thermally nucleate and grow at a high temperature of 550 °C. The interface between the precipitates and the matrix gradually loses the coherency generating new open-volume defects [30,44]. The positrons can be trapped by the misfit and annihilate with the surrounding Au/Cu precipitates, resulting in the enhancement of *W* parameters.

The *S*–*W* plots reflect energy-dependent evolution of the correlation between the precipitation and the generation of irradiation-induced defects. As shown in Fig. 3, the (*S, W*) points for the unirradiated samples follow a single linear relationship (labelled as L_0): *S* decreases and *W* increases with increasing positron energy. The slope of the linear *S*–*W* dependence for the unirradiated Fe–Au and Fe–Cu alloy samples is almost the same as that of the unirradiated pure Fe sample, suggesting that positrons were annihilated randomly in the homogenised materials (predominantly in the vicinity of the Fe atoms). The *S*–*W* plot for the irradiated samples cannot be represented by a single straight line, indicating that new types of defects were introduced by the He implantation. For all three materials, the evolution of (*S, W*) points can be divided into three (linear) segments with lines labelled L_1, L_2 and L_3, respectively, for variable energies representative for a mean positron depth ranging from the surface to the bulk. For the irradiated pure Fe sample (Fig. 3(a)), the slope of segment L_1 in region I

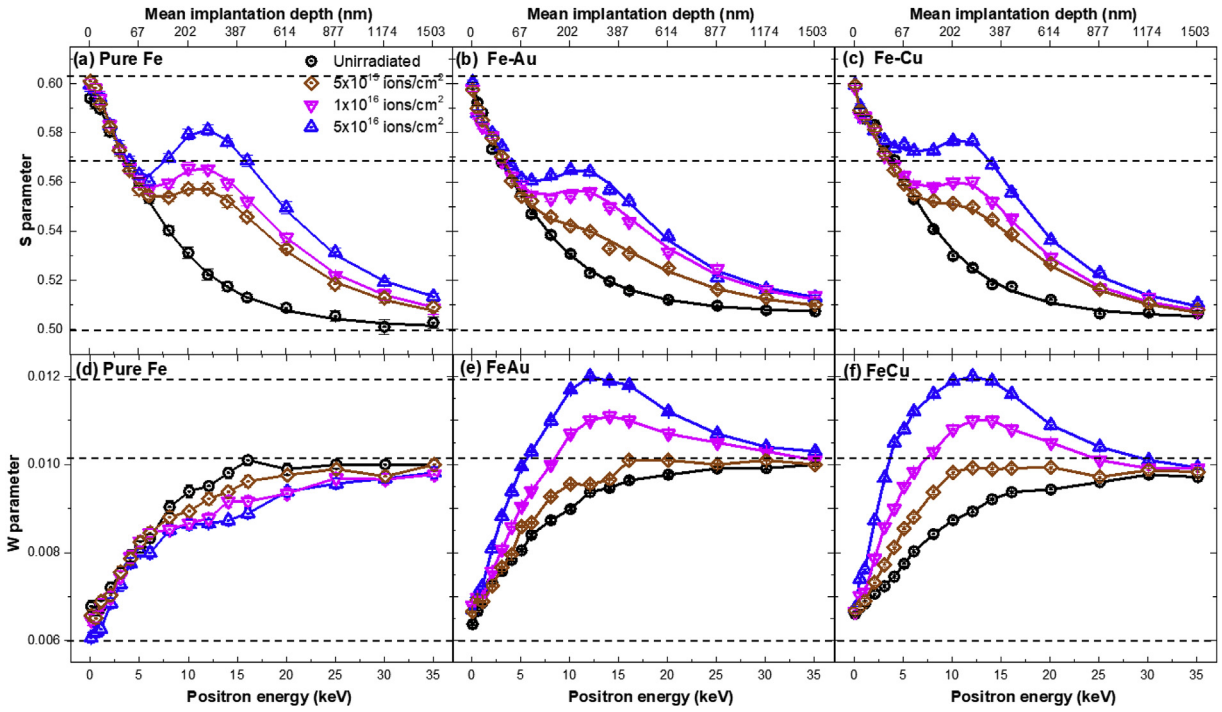

Fig. 2. Dependence of (a–c) *S(E)* curves and (d–f) *W(E)* curves on irradiation fluences for pure Fe, Fe–Au alloy and Fe–Cu alloy samples. For comparison, the *S(E)* and *W(E)* curves for the unirradiated samples are included.

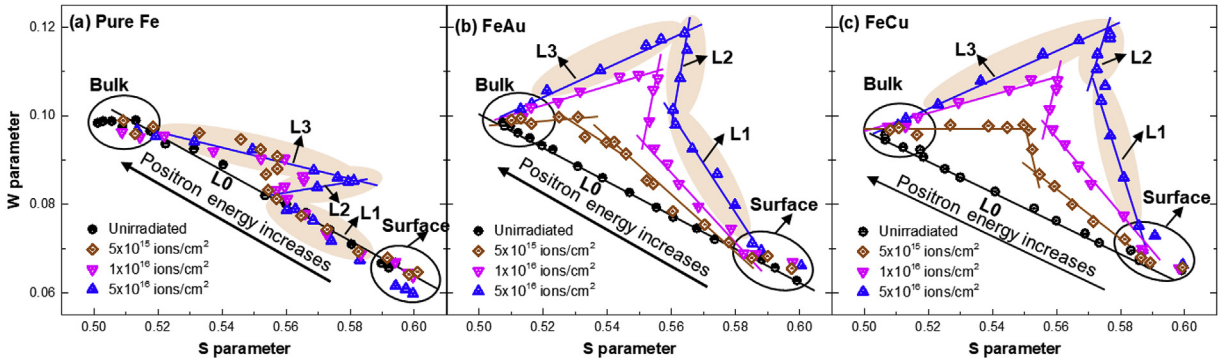

Fig. 3. *S–W* plots for (a) pure Fe, (b) Fe–Au and (c) Fe–Cu alloy samples for unirradiated and irradiated with different fluences.

is the same as that of the unirradiated sample, indicating that positrons are predominantly annihilated with the Fe electrons. At increasing depth values, the implanted He ions diffuse into the matrix and are easily trapped by vacancies, forming He_mV_n complexes, as a result of the extremely low solubility of helium in metals [45] in combination with the high binding energy between He and vacancies [46]. The positron annihilation with He electrons results in a change in slope for segment L_2 in region II. For segment L_3 in region III (depth >200 nm), the ratio of helium atoms to vacancies increases and more helium atoms are trapped by He_mV_n complexes, forming He filled cavities [47].

For the irradiated samples, the difference in evolution of the (*S*, *W*) data of the Fe–Au and Fe–Cu alloys samples, with that of irradiated pure Fe is obvious. For region I, the slope of L_1 differs from that of L_0, which is due to the interaction of Cu and Au solutes with vacancies. In region II, the aligned lines L_2 are parallel for the samples irradiated with 5.0×10^{16} and 1.0×10^{16} ions/cm^2. However, the slope of L_2 for low irradiation doses is obviously different, which might result from the decrease in the fraction of positrons annihilated with solute electrons. In region III, the *S* parameters decrease as the increasing of penetration depth coupled with a decrease of the *W* parameters. This suggests that the chemical environment around the cavities changes as a result of the irradiation at an elevated temperature.

The *S* and *W* parameters for the irradiated samples were normalized to those of the respective unirradiated samples in order to extract more specific information related to the nature of the vacancy-like defects and precipitates [26,30]. As shown in Fig. 4(a), the normalized *S* values (S_{Nor}) for the irradiated pure Fe samples shows a maximum value at a depth corresponding to the maximum dpa position (about 350 nm) calculated by SRIM. Similar phenomena are observed for the irradiated Fe–Au and Fe–Cu alloys samples, (see Fig. 4(b) and 4(c)). The amplitude of the S_{Nor} increases as the irradiation dose increases whereas the peak position does not shift. The normalized *W* parameter (W_{Nor}) exhibits a broad valley for the irradiated pure Fe sample (Fig. 4(d)) and the lowest value of the valley is located at the same position as the peak of the S_{Nor} (Fig. 4(a)). For the pure Fe sample the decrease in W_{Nor} mainly

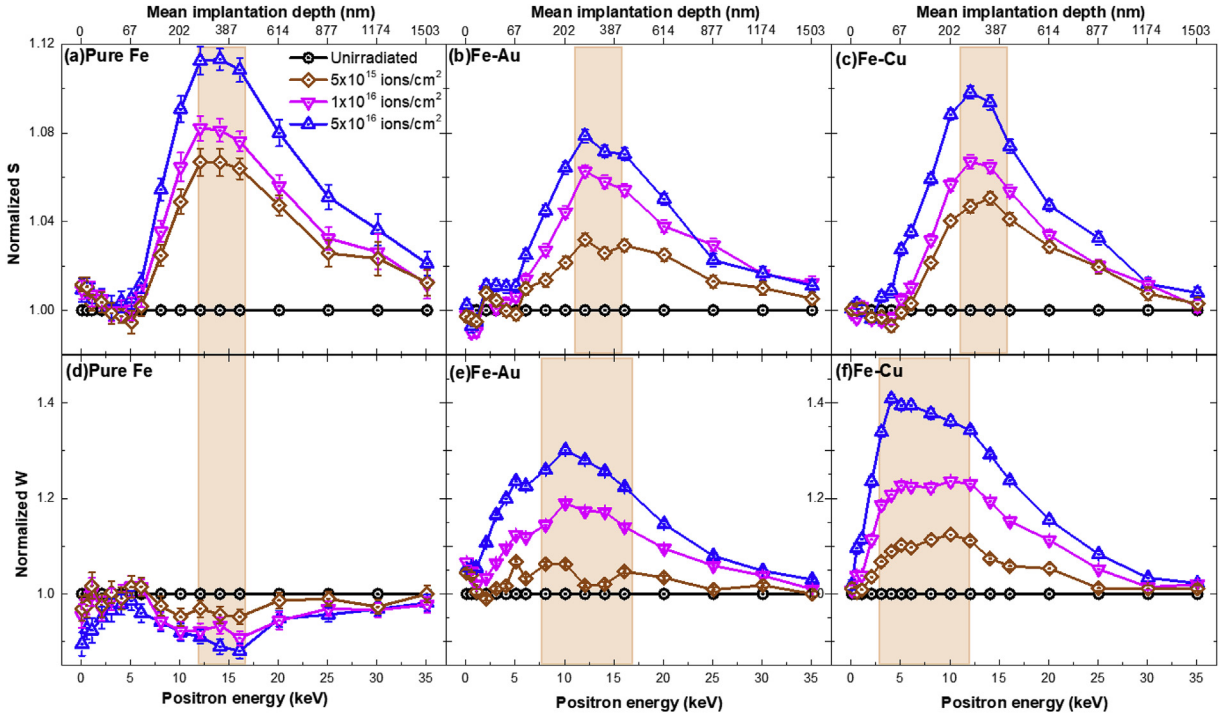

Fig. 4. Dependence of (a–c) normalized *S* parameter and (d–f) normalized *W* parameters on positron energy with different fluences for the pure Fe, the Fe–Au alloy and the Fe–Cu alloy samples. For comparison, the evolution of the normalized *S* and *W* parameters for the unirradiated samples are also included.

results from the corresponding increase in S_{Nor} since the enhanced annihilation at vacancy-like defects reduces the relative contribution from annihilations in bulk Fe [26]. In contrast, a broad peak in the W_{Nor} curve is observed for the irradiated Fe–Au and Fe–Cu alloys samples. The amplitude of the peak increases with an increasing irradiation dose, confirming an accelerated precipitation by irradiation.

For the Fe–Au alloy samples, the maximum damage region reflected by a maximum in S_{Nor} (shaded in Fig. 4(b)), coincides with the region where W_{Nor} reached a maximum (shaded in Fig. 4(e)), demonstrating a close correlation between the vacancy-like defects and the Au solute. Since the positron affinity of Au is lower than that of vacancy-like defects [28,43], positrons prefer to be trapped by vacancy-like defects. The increase in W_{Nor} corresponds to the presence of Au clusters or precipitates that decorate the open volume defects and the formation of Au-vacancy complexes. In contrast, the maximum W_{Nor} for the irradiated Fe–Cu alloy samples is found at lower incident positron energies, (shaded in Fig. 4(f)), compared to the peak regions for S_{Nor} (shaded in Fig. 4(b)). It implies a weak correlation between the vacancy-like defects and the Cu solute.

In order to compare the degree of radiation damage in pure Fe with Fe–Au and Fe–Cu alloys, the *S* parameters normalized by the unirradiated pure Fe as a function of the positron energy are grouped per fluence level. Although the normalized *S* parameters cannot quantify the radiation swelling, a reduction in the *S* parameter is positively correlated in a non-linear manner with the void swelling [48]. As shown in Fig. 5, in the unirradiated samples, the effect of solute Au or Cu atoms on the S_{Nor}-*E* curves is negligible. For a given fluence the normalized *S* parameters of the irradiated Fe–Au and Fe–Cu alloy samples are significantly lower than those of the pure Fe sample. Moreover, the S_{Nor} values for the Fe–Au sample are lower than those of the Fe–Cu samples for all three doses in particular in the range from 5 to 20 keV. This observation suggests a superior radiation resistance to swelling in the Fe–Au alloy compared to the Fe–Cu alloy.

3.3. Transmission electron microscopy

Fig. 6 presents bright field TEM images which reveal irradiation-induced defects in pure Fe after a fluence of 5.0×10^{16} ions/cm^2. In the subsurface region (<200 nm), a high density of micro-voids is observed (Fig. 6(a)). In the maximum damage region, cavities are formed (Fig. 6(b) and 6(c)). Besides some spherical cases, many of the cavities were faceted with square or hexagonal shapes. A significant variation in cavity size ranging from around 3 to 15 nm is observed.

Fig. 7(a) presents a TEM micrograph showing the presence of cavities and Au precipitates from the implanted surface to a depth of about 500 nm after irradiation up to a fluence of 1.0×10^{16} ions/cm^2. To clarify the correlation between Au precipitates and the irradiation-induced damage, the elemental Au distribution of the same region is shown in Fig. 7(b). A high density of spherical cavities can be clearly observed at a depth >200 nm, which corresponds to region III in the *S*–*W* plot. At a depth below 200 nm, the observed degree of the radiation damage is low. Au precipitates are mainly formed as large particles along the grain boundaries and some discs in the matrix. One region indicated by a red rectangle in Fig. 7(a) is shown in Fig. 7(c) at higher magnification. The elemental mapping of Au confirms a strong site correlation of Au precipitates with radiation-induced cavities.

The microstructure of the Fe–Cu alloy after irradiation up to a dose of 1.0×10^{16} ions/cm^2 is shown in Fig. 8. Spherical cavities are observed at a depth of 300–600 nm, which agrees well with the inferred defect type in region III on the basis of the *S*–*W* results. Fig. 8(b) shows details of the cavities at higher magnification in the region indicated by the rectangle shown in Fig. 8(a). A high density of micro-voids can be observed in the region close to the surface (Fig. 8(c)), corresponding to region I in the *S*–*W* plot in Fig. 3. A HAADF mode micrograph is shown in Fig. 8(d) with the corresponding Cu elemental map presented in Fig. 8(e). The location of the cavities is also indicated by red circles to reveal the absence or

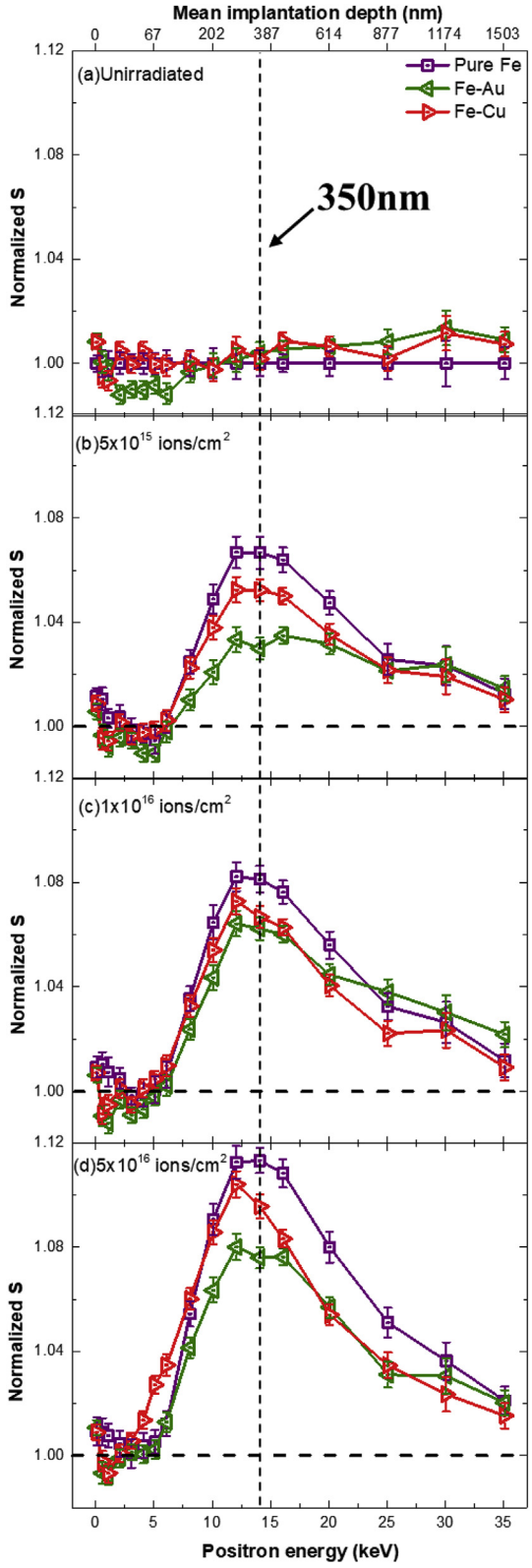

Fig. 5. Comparison of the *S(E)* curves for the pure Fe, Fe–Au alloy and Fe–Cu alloy samples: (a) unirradiated and irradiated by He^+ ions up to a fluence of (b) 5.0×10^{15} ions/cm^2, (c) 1.0×10^{16} ions/cm^2 and (d) 5.0×10^{16} ions/cm^2.

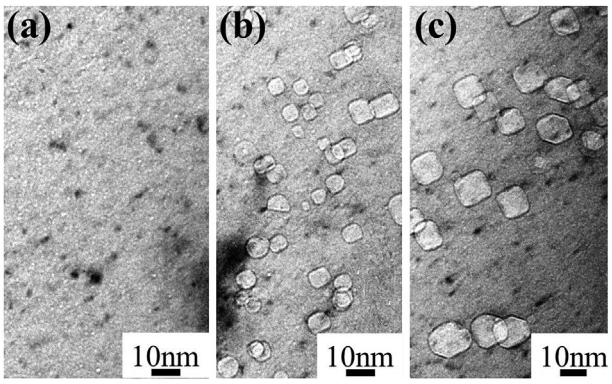

Fig. 6. Bright field TEM image of pure Fe after irradiation of 5.0×10^{16} ions/cm^2 with a depth of (a) < 200 nm, (b) 200–300 nm and (c) 300–400 nm.

presence of a site correlation between the cavities and the precipitates. Even though some Cu precipitates are observed close to the cavities, most nano-size Cu precipitates are homogeneously formed in the Fe matrix at locations without detectable radiation damage. The reduced tendency for Cu solutes to segregate to topological defects has also been observed in earlier high temperature mechanical deformation experiments using binary Fe–Cu alloys of comparable composition [30,49].

3.4. *Ab initio calculations*

As shown experimentally, the introduction of dissolved Au and Cu atoms in the matrix can significantly reduce the irradiation swelling behaviour of Fe-based materials, by the precipitation of Au (and to a lesser extent of Cu) in radiation-induced open volume defects, such as vacancies, vacancy clusters and He filled cavities. More importantly, Fe–Au exhibits a superior radiation swelling resistance in comparison to Fe–Cu. Previous *Ab-initio* calculations showed that the diffusivity of Au in *bcc* Fe is more than one order of magnitude faster than *bcc* Fe self-diffusion, while the diffusivity of Cu is comparable with Fe self-diffusion [50]. The fast diffusion of solute Au facilitates the Au segregation and precipitation process, which can be further enhanced with a high concentration of vacancies generated by irradiation. To elucidate the origin of correlation between Au/Cu precipitates and irradiation-induced defects, we computationally examine the interaction of the solute Au and Cu atoms with these open volume defects using *ab initio* calculations. The interaction of solute Au and Cu atoms with the monovacancy (*V*) and substitutional He (*He*) has been extensively studied. The binding energy of *Au–V* and *Au–He* are 0.46 eV [39] and 0.56 eV [32], respectively, which are slightly larger than that of solute Cu (0.28 eV for the *Cu–V* [39] and 0.30 eV for *Cu-He* [22], respectively). Such a small difference cannot explain the obtained experimental results. Apparently, various Au_k-He_m-V_n and Cu_k-He_m-V_n can exist in practice and their behaviors are very complex. In the present calculations, we only focus on two simple cases, i.e., only one solute Au or Cu atom in the vacancy clusters, *Au-Vn* and *Cu-Vn,* and only one solute Au or Cu atom in the vacancies-He complexes with $He/V = 1$, *Au-*He_n-V_n and *Cu-*He_n-V_n, in order to qualitatively understand the above experimental phenomenon.

Firstly, to verify the validity of our *ab-initio* calculations, we have calculated the monovacancy formation energy (E_f^V), the binding energy of vacancy to a vacancy cluster (V_n) consisting of *n* vacancies ($E_b^{V-V_{n-1}}$) in iron, as well as the binding energies of *Au–V* (E_b^{Au-V}), *Au–He* (E_b^{Au-He}), *Cu–V* (E_b^{Cu-V}), and *Cu–He* (E_b^{Cu-He}). The results are listed in Table 2. Previously published values for these parameters are also included in the table for comparison. Our calculated

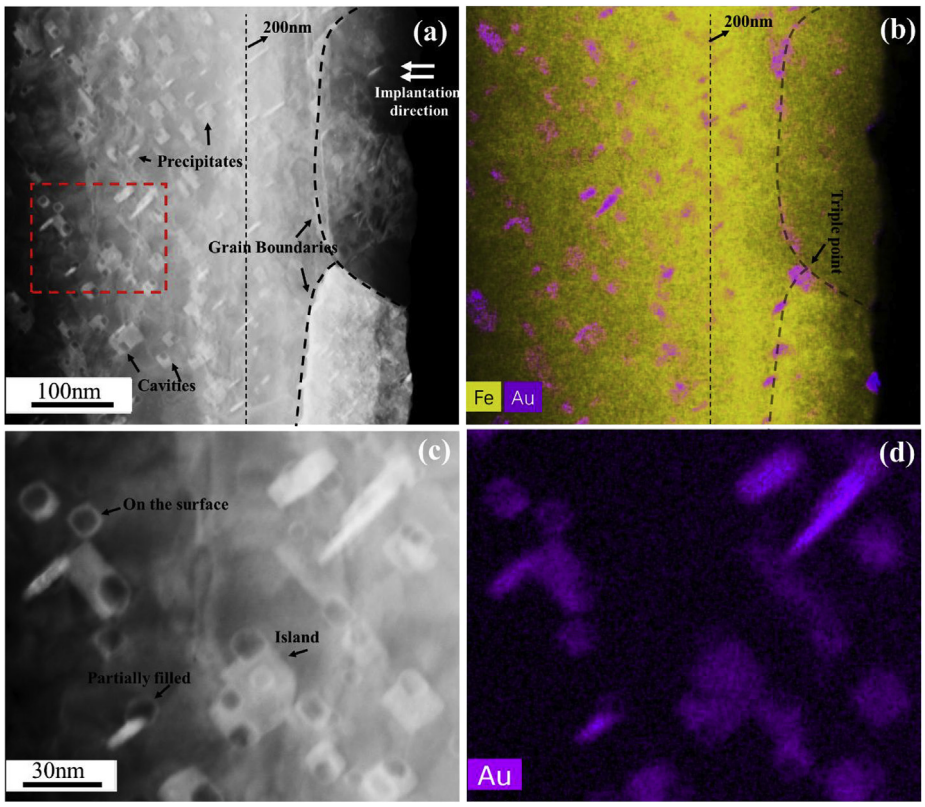

Fig. 7. (a) HAADF mode image of the Fe–Au alloy samples after He^+ irradiation (550 °C, 1.0×10^{16} ions/cm^2) for a region from surface to around 500 nm depth; (b) corresponding elemental mapping (Fe and Au) of the region shown in the panel (a); (c) the region indicated in the panel (b) by red dashed rectangle shown in higher magnification; (d) elemental mapping (Au) of the region shown in the panel (c). (For interpretation of the references to colour in this figure legend, the reader is referred to the Web version of this article.)

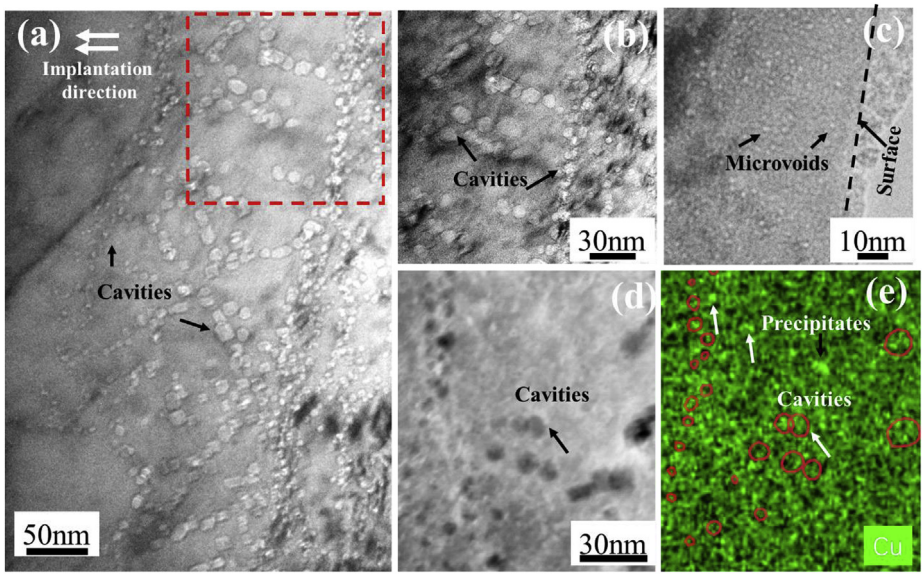

Fig. 8. (a) Bright field TEM of the Fe–Cu alloy samples after He^+ irradiation (550 °C, 1.0×10^{16} ions/cm^2) in depth of 300–600 nm with an enlargement image in (b); (c) bright field TEM within a depth of around 100 nm; (d) HAADF mode image of Fe–Cu alloy samples after He^+ irradiation (550 °C, 1.0×10^{16} ions/cm^2). (e) elemental mapping (Cu) of the region shown in the panel (d).

vacancy formation energy in Fe is 2.14 eV, which is in good agreement with previous *ab initio* calculations [33]. Regarding the binding energies of *Cu–V, Cu–He, Au–V,* and *Au–He*, our data closely resemble the previously reported values. The difference between the present values and those from previous studies is due to the use of a different cell relaxation method. In our work, both the supercell volume and shape are fully relaxed, i.e., a constant pressure condition is imposed, whereas the previous studies were done at constant volume [22,32,39]. Note that the results computed at constant pressure and volume have a better consistency for Cu-

Table 2
Monovacancy formation energy (E_f^V), vacancy cluster (V_n) binding energies ($E_b^{V-V_{n-1}}$), as well as the binding energies of complexes *Cu*–*V* (E_b^{Cu-V}), *Au*–*V* (E_b^{Au-V}), *Cu*–*He* (E_b^{Cu-He}) and *Au*–*He* (E_b^{Au-He}).

	E_f^V	E_b^{V-V}	$E_b^{V-V_2}$	$E_b^{V-V_3}$	E_b^{Au-V}	E_b^{Au-He}	E_b^{Cu-V}	E_b^{Cu-He}
This work	2.14	0.22	0.41	0.72	0.38	0.47	0.24	0.30
Literature	2.17 [33]	0.28 [51]	0.36 [51]	0.70 [51]	0.46 [39]	0.56 [32]	0.28 [39]	0.30 [22]

related defects than those for Au-related defects. This might be due to a higher atomic size factor for Au [31].

Fig. 9 presents the calculated binding energies of solute Au and Cu with V_n as well as He_n-V_n. Fig. 10 presents the initial and final stable configurations of solute Au and Cu in V_n for $n \geq 2$. To obtain their most stable configurations, we constructed a series of *Au*-V_n and *Cu*-V_n complexes, where an Au or Cu atom is inserted at the core of V_n cluster or replaces a Fe atom in the vicinity of V_n cluster. In each case, we examined about a dozen configurations after considering the symmetry. All these calculations are performed at constant pressure, i.e., the relaxations of atomic and optimizations of the shape and size of the supercell are allowed.

As shown in Fig. 9, positive binding energies indicate that both solute Au and Cu atoms can be trapped by vacancy-like defects, and therefore lead to Cu/Au segregation and precipitation at those defects. This is consistent with the experimental observations described in section 3.2 and 3.3. For pure vacancies, the binding energy of *Au*-V_n increase rapidly from 0.38 to 1.56 eV as the vacancy cluster size n increases from 1 to 5. On the other hand, the binding energy of *Cu*-V_n increases more moderately from 0.24 to 0.56 eV when n increases from 1 to 5 and become insensitive to the vacancy cluster size when $n > 3$. It is obvious that the binding energies of *Au*-V_n are much larger than those of *Cu*-V_n, indicating that the trapping capability of a vacancy cluster for solute Au atoms is much stronger than that for solute Cu atoms. The binding energies of *Au*-He_n-V_n are significantly lower than those of *Au*-V_n for $n \geq 2$. This suggests that He weakens the trapping capability of a vacancy for solute Au atoms. In contrast, the introduction of helium into vacancy clusters can slightly enhance the trapping capability of a vacancy cluster for solute Cu atoms. The binding energies of *Cu*-He_n-V_n are slightly larger than those of *Cu*-V_n. Nevertheless, the trapping of solute Au atoms by vacancy clusters filled with He atoms is till stronger than

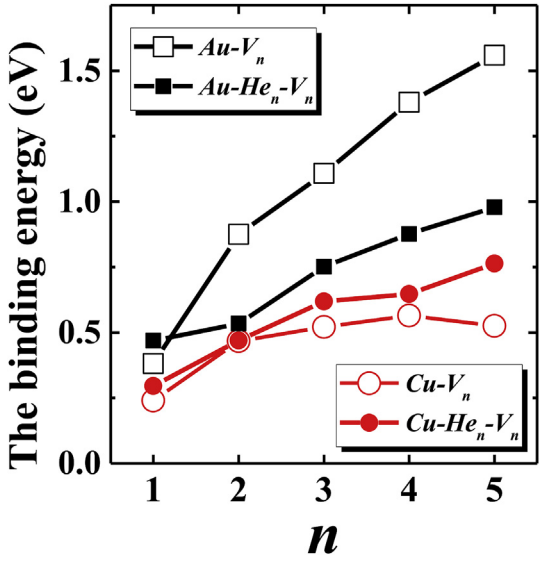

Fig. 9. Binding energies of complexes *Au*-V_n ($E_b^{Au-V_n}$), *Cu*-V_n ($E_b^{Cu-V_n}$), *Au*-He_nV_n ($E_b^{Au-He_nV_n}$) and *Cu*- He_nV_n ($E_b^{Cu-He_nV_n}$) plotted as a function of the vacancy cluster size n.

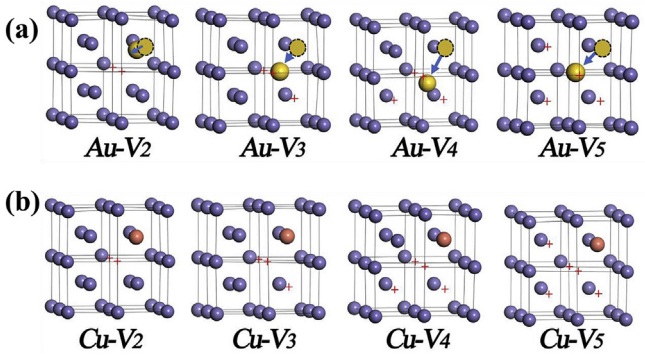

Fig. 10. The most stable configuration of solute Au and Cu in V_n for $n \geq 2$. The Fe, Au and Cu are denoted by purple, yellow and red balls, respectively. The vacancy sites are denoted by red "+". (For interpretation of the references to colour in this figure legend, the reader is referred to the Web version of this article.)

that for solute Cu atoms. This explains why Au precipitates more closely linked to vacancy-like defects than Cu precipitates. The difference in behaviour of Au and Cu in vacancy clusters is also reflected in their calculated equilibrium configurations. As shown in Fig. 10, the solute Au atom spontaneously moves from the lattice position nearby the vacancy cluster to the core region of V_n when $n > 2$ after complete relaxation, whereas solute Cu atom always occupies the lattice position nearby V_n during the relaxation, i.e., the lattice position nearby V_n is the most stable site for solute Cu atoms. This is consistent with the experimental observations.

These differences in vacancy cluster trapping between Au and Cu solutes could be attributed to the different atomic size of the Au and Cu atoms. The atomic volume of Au is much larger than that of Fe. The introduction of an Au atom in the Fe lattice will cause a severe lattice distortion (the relative volume difference, known as the size factor, of Au in bcc Fe is $\Omega_{sf}^{Au} = 0.44$ [31]). Therefore, when the Au atom is near the vacancy cluster, it tends to relax toward the core of the vacancy cluster in order to relieve the misfit strain. In contrast, the atomic volume of Cu is close to that of Fe. The introduction of Cu atoms in the Fe lattice matrix does not cause obvious lattice distortion (the volume size factor of Cu in bcc Fe is $\Omega_{sf}^{Cu} = 0.18$ [31]). On the other hand, as shown in Fig. 11, the electronic interactions of both Au and Cu with Fe are very weak due to their full *d*-shell. Therefore, the Au atoms prefer to occupy the center of the vacancy, whereas the Cu atoms prefer to occupy the lattice sites around the vacancy cluster. Furthermore, the bigger the vacancy cluster, the larger the space available for Au occupation. Thus, the binding energy of *Au*-V_n increases with the vacancy cluster size.

4. Conclusions

Pure Fe and binary Fe–Au and Fe–Cu model alloys were irradiated with helium ions at 550 °C with fluences of 5.0×10^{15}, 1.0×10^{16} and 5.0×10^{16} ions/cm^2, respectively, to investigate the influence of precipitation on the evolution of irradiation-induced defects. Variable energy positron annihilation spectroscopy and TEM measurements are performed to characterize both the

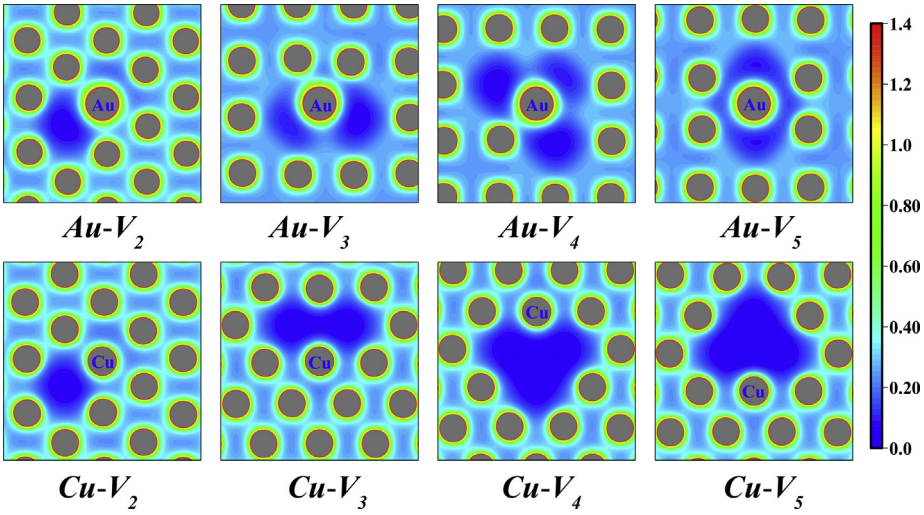

Fig. 11. Charge density map for stable *Au-V*$_n$ and *Cu-V*$_n$. The units are $e/Å^3$. To demonstrate the electronic interaction with the closest Fe atoms, the plane shown for *Au−V*$_2$ and *Cu-V*$_n$ is (110) whereas the plane for *Au−V*$_3$, *Au−V*$_4$, *Au−V*$_5$ is (100).

radiation damage and precipitates to study their site correlation. The origin of the difference in healing behaviour for Fe—Cu and Fe—Au alloys is clarified by *ab initio* calculations. The main conclusions are as follows:

(1) The formation of vacancy-like defects is promoted with increasing irradiation fluences. The normalized *S* parameters for the Fe—Au and Fe—Cu model alloys are reduced compared to those for pure Fe. Lower normalized *S* parameter values are found for the Fe—Au alloy in comparison to the Fe—Cu alloy, suggesting a reduced radiation swelling.
(2) Both the Au and Cu precipitation are accelerated by irradiation, as indicated by an increase in *W* parameters with the increasing irradiation fluences. A close spatial correlation of Au precipitates with the irradiation-induced defects is found whereas the Cu precipitation and the radiation damage are only weakly inter-related.
(3) *Ab initio* calculations indicate a high binding energy between Au solutes and vacancies. The energetically most favourable positions of Au atoms in pure vacancy clusters are located in the core region of the vacancy clusters, whereas Cu atoms always prefer to occupy the lattice sites around the vacancy cluster. Even though He atoms can weaken the trapping capability of vacancy to solute Au, the trapping of vacancy cluster filled with He by solute Au atoms remains stronger than that for solute Cu atoms.

Declaration of competing interest

The authors declare that they have no known competing financial interests or personal relationships that could have appeared to influence the work reported in this paper.

Acknowledgements

This research was supported by the National Natural Science Foundation of China (Grant No. 51701095, 51771185), the Natural Science Foundation of Jiangsu Province, China (Grant No. BK20170798) and the Technology Agency of the Czech Republic (project No. TK01030153). We thank Weiping Zhang for the radiation experiments and Mingda Sun for fruitful discussion and assistance during the TEM experiments.

References

[1] P.P. Liu, Q. Zhan, Z.Y. Fu, Y.P. Wei, Y.M. Wang, F.M. Wang, S. Ohnuki, F.R. Wan, Surface and internal microstructure damage of He-ion-irradiated CLAM steel studied by cross-sectional transmission electron microscopy, J. Alloy. Comp. 649 (2015) 859—864, https://doi.org/10.1016/j.jallcom.2015.07.177.
[2] S.J. Zinkle, G.S. Was, Materials challenges in nuclear energy, Acta Mater. 61 (2013) 735—758, https://doi.org/10.1016/j.actamat.2012.11.004.
[3] R. Gao, B. Cheng, L.F. Zeng, S. Miao, J. Hou, T. Zhang, X.P. Wang, Q.F. Fang, C.S. Liu, Microstructure, hardness and defect structure of the He irradiated ODS ferritic steel, J. Alloy. Comp. 691 (2017) 653—658, https://doi.org/10.1016/j.jallcom.2016.08.312.
[4] G. Ackland, Controlling radiation damage, Science 327 (2010) 1587—1588, https://doi.org/10.1126/science.1188088.
[5] K.S. Toohey, N.R. Sottos, J.A. Lewis, J.S. Moore, S.R. White, Self-healing materials with microvascular networks, Nat. Mater. 6 (2007) 581—585, https://doi.org/10.1038/nmat1934.
[6] V.K. Thakur, M.R. Kessler, Self-healing polymer nanocomposite materials: a review, Polymer 69 (2015) 369—383, https://doi.org/10.1016/j.polymer.2015.04.086.
[7] W.G. Sloof, R. Pei, S.A. McDonald, J.L. Fife, L. Shen, L. Boatemaa, A.-S. Farle, K. Yan, X. Zhang, S. van der Zwaag, P.D. Lee, P.J. Withers, Repeated crack healing in MAX-phase ceramics revealed by 4D in situ synchrotron X-ray tomographic microscopy, Sci. Rep. 6 (2016) 1—9, https://doi.org/10.1038/srep23040.
[8] T. Ouyang, J. Wu, M. Yasir, T. Zhou, X. Fang, Y. Wang, D. Liu, J. Suo, Effect of TiC self-healing coatings on the cyclic oxidation resistance and lifetime of thermal barrier coatings, J. Alloy. Comp. 656 (2016) 992—1003, https://doi.org/10.1016/j.jallcom.2015.07.271.
[9] K. Van Tittelboom, N. De Belie, Self-healing in cementitious materials-A review, Materials 6 (2013) 2182—2217, https://doi.org/10.3390/ma6062182.
[10] M.D. Hager, P. Greil, C. Leyens, S. van der Zwaag, U.S. Schubert, Self-healing materials, Adv. Mater. 22 (2010) 5424—5430, https://doi.org/10.1002/adma.201003036.
[11] N. van Dijk, S. van der Zwaag, Self-healing phenomena in metals, Adv. Mater. Interfaces 5 (2018), https://doi.org/10.1002/admi.201800226.
[12] X.M. Bai, A.F. Voter, R.G. Hoagland, M. Nastasi, B.P. Uberuaga, Efficient annealing of radiation damage near grain boundaries via interstitial emission, Science 327 (2010) 1631—1634, https://doi.org/10.1126/science.1183723.
[13] X. Li, W. Liu, Y. Xu, C.S. Liu, B.C. Pan, Y. Liang, Q.F. Fang, J.-L. Chen, G.N. Luo, G.-H. Lu, Z. Wang, Radiation resistance of nano-crystalline iron: coupling of the fundamental segregation process and the annihilation of interstitials and vacancies near the grain boundaries, Acta Mater. 109 (2016) 115—127, https://doi.org/10.1016/j.actamat.2016.02.028.
[14] Y. Zhang, D. Schwen, Y. Zhang, X.-M. Bai, Effects of oversized tungsten on the primary damage behavior in Fe-W alloys, J. Alloy. Comp. 794 (2019) 482—490, https://doi.org/10.1016/j.jallcom.2019.04.278.
[15] V. Borovikov, X.-Z. Tang, D. Perez, X.-M. Bai, B.P. Uberuaga, A.F. Voter, Coupled motion of grain boundaries in bcc tungsten as a possible radiation-damage healing mechanism under fusion reactor conditions, Nucl. Fusion 53 (2013), https://doi.org/10.1088/0029-5515/53/6/063001.
[16] J. Li, K.Y. Yu, Y. Chen, M. Song, H. Wang, M.A. Kirk, M. Li, X. Zhang, In situ study of defect migration kinetics and self-healing of twin boundaries in heavy ion irradiated nanotwinned metals, Nano Lett. 15 (2015) 2922—2927, https://doi.org/10.1021/nl504677z.

[17] R.A. Johnson, N.Q. Lam, Solute segregation in metals under irradiation, Phys. Rev. B (Solid State) 13 (1976) 4364–4375, https://doi.org/10.1103/PhysRevB.13.4364.
[18] N.Q. Lam, P.R. Okamoto, H. Wiedersich, Effects of solute segregation and precipitation on void swelling in irradiated alloys, J. Nucl. Mater. 74 (1978) 101–113, https://doi.org/10.1016/0022-3115(78)90538-x.
[19] J. Weertman, D.M. Parkin, Suppression of irradiation swelling through an impurity-point defect trapping mechanism involving reduction of the dislocation bias factor, J. Nucl. Mater. 99 (1981) 66–74, https://doi.org/10.1016/0022-3115(81)90139-2.
[20] A.C. Arokiam, A.V. Barashev, D.J. Bacon, Y.N. Osetsky, Simulation of copper atom diffusion via the vacancy mechanism in a dilute Fe-Cu alloy, Phys. Rev. B 71 (2005), https://doi.org/10.1103/PhysRevB.71.174205.
[21] A.C. Arokiam, A.V. Barashev, D.J. Bacon, Y.N. Osetsky, Atomic-scale computer simulation study of the interaction of Cu-rich precipitates with irradiation-produced defects in alpha-Fe, Philos. Mag. 87 (2007) 925–943, https://doi.org/10.1080/14786430601003908.
[22] J.X. Yan, Z.X. Tian, W. Xiao, W.T. Geng, Interaction of He with Cu, V, and Ta in bcc Fe: a first-principles study, J. Appl. Phys. 110 (2011), https://doi.org/10.1063/1.3602156.
[23] C. Domain, C.S. Becquart, Ab initio calculations of defects in Fe and dilute Fe-Cu alloys, Phys. Rev. B 65 (2002), https://doi.org/10.1103/PhysRevB.65.024103.
[24] Y. Nagai, Z. Tang, M. Hassegawa, T. Kanai, M. Saneyasu, Irradiation-induced Cu aggregations in Fe: an origin of embrittlement of reactor pressure vessel steels, Phys. Rev. B 63 (2001), https://doi.org/10.1103/PhysRevB.63.134110.
[25] J. Čížek, I. Procházka, J. Kocik, The clustering of Cu atoms in neutron irradiated reactor pressure vessel steels studied by positron annihilation, in: A. Ochsner, G.E. Murch (Eds.), Diffusion in Solids and Liquids III, Trans Tech Publications, Switzerland, 2008, pp. 81–86.
[26] S. Jin, P. Zhang, E. Lu, L. Guo, B. Wang, X. Cao, Correlation between Cu precipitates and irradiation defects in Fe-Cu model alloys investigated by positron annihilation spectroscopy, Acta Mater. 103 (2016) 658–664, https://doi.org/10.1016/j.actamat.2015.10.051.
[27] S. Jin, X. Lian, T. Zhu, Y. Gong, P. Zhang, X. Cao, R. Yu, B. Wang, Irradiation evolution of Cu precipitates in Fe1.0Cu alloy studied by positron annihilation spectroscopy, J. Nucl. Mater. 499 (2018) 65–70, https://doi.org/10.1016/j.jnucmat.2017.11.011.
[28] Q. Xu, T. Yoshiie, K. Sato, Dose dependence of Cu precipitate formation in Fe-Cu model alloys irradiated with fission neutrons, Phys. Rev. B 73 (2006), https://doi.org/10.1103/PhysRevB.73.134115.
[29] Q. Xu, T. Yoshiie, Effects of damage rate on Cu precipitation in Fe-Cu model alloys under neutron irradiation, Philos. Mag. 91 (2011) 3716–3726, https://doi.org/10.1080/14786435.2011.590459.
[30] S.M. He, N.H. van Dijk, H. Schut, E.R. Peekstok, S. van der Zwaag, Thermally activated precipitation at deformation-induced defects in Fe-Cu and Fe-Cu-B-N alloys studied by positron annihilation spectroscopy, Phys. Rev. B 81 (2010), https://doi.org/10.1103/PhysRevB.81.094103.
[31] H. King, Quantitative size-factors for metallic solid solutions, J. Mater. Sci. 1 (1966) 79–90, https://doi.org/10.1007/bf00549722.
[32] W. Hao, W.T. Geng, Gold might slow down the growth of helium bubble in iron, Nucl. Instrum. Methods Phys. Res., Sect. B 269 (2011) 1428–1430, https://doi.org/10.1016/j.nimb.2011.04.007.
[33] T. Ohnuma, N. Soneda, M. Iwasawa, First-principles calculations of vacancy-solute element interactions in body-centered cubic iron, Acta Mater. 57 (2009) 5947–5955, https://doi.org/10.1016/j.actamat.2009.08.020.
[34] Q. Cao, X. Ju, L. Guo, B. Wang, Helium-implanted CLAM steel and evolutionary behavior of defects investigated by positron-annihilation spectroscopy, Fusion Eng. Des. 89 (2014) 1101–1106, https://doi.org/10.1016/j.fusengdes.2013.11.008.
[35] G. Kresse, J. Furthmuller, Efficient iterative schemes for ab initio total-energy calculations using a plane-wave basis set, Phys. Rev. B 54 (1996) 11169–11186, https://doi.org/10.1103/PhysRevB.54.11169.
[36] P.E. Blöchl, Projector augmented-wave method, Phys. Rev. B 50 (1994) 17953–17979, https://doi.org/10.1103/PhysRevB.50.17953.
[37] J.P. Perdew, K. Burke, M. Ernzerhof, Generalized gradient approximation made simple, Phys. Rev. Lett. 77 (1996) 3865–3868, https://doi.org/10.1103/PhysRevLett.77.3865.
[38] R.W.G. Wyckoff, Crystal Structures, Interscience, Krieger, 1964.
[39] P. Olsson, T.P.C. Klaver, C. Domain, Ab initio study of solute transition-metal interactions with point defects in bcc Fe, Phys. Rev. B 81 (2010), https://doi.org/10.1103/PhysRevB.81.054102.
[40] J.F. Ziegler, M.D. Ziegler, J.P. Biersack, SRIM - the stopping and range of ions in matter, Nucl. Instrum. Methods Phys. Res., Sect. B 268 (2010) (2010) 1818–1823, https://doi.org/10.1016/j.nimb.2010.02.091.
[41] J.D. Hunn, E.H. Lee, T.S. Byun, L.K. Mansur, Ion-irradiation-induced hardening in inconel 718, J. Nucl. Mater. 296 (2001) 203–209, https://doi.org/10.1016/s0022-3115(01)00519-0.
[42] R.E. Stoller, M.B. Toloczko, G.S. Was, A.G. Certain, S. Dwaraknath, F.A. Garner, On the use of SRIM for computing radiation damage exposure, Nucl. Instrum. Methods Phys. Res., Sect. B 310 (2013) 75–80, https://doi.org/10.1016/j.nimb.2013.05.008.
[43] M.J. Puska, P. Lanki, R.M. Nieminen, Positron affinities for elemental metals, J. Phys. Condens. Matter 1 (1989) 6081–6095, https://doi.org/10.1088/0953-8984/1/35/008.
[44] S. Zhang, H. Schut, J. Čížek, F. Tichelaar, E. Brück, S. van der Zwaag, N.H. van Dijk, Positron annihilation study on deformation-induced Au precipitation in Fe-Au and Fe-Au-B-N alloys, J. Mater. Sci. 49 (2014) 2509–2518, https://doi.org/10.1007/s10853-013-7946-9.
[45] H. Ullmaier, The influence of helium on the bulk properties of fusion reactor structural materials, Nucl. Fusion 24 (1984) 1039–1083, https://doi.org/10.1088/0029-5515/24/8/009.
[46] C.C. Fu, F. Willaime, Ab initio study of helium in alpha-Fe: dissolution, migration, and clustering with vacancies, Phys. Rev. B 72 (2005), https://doi.org/10.1103/PhysRevB.72.064117.
[47] M. Cui, C. Yao, T. Shen, L. Pang, Y. Zhu, B. Li, X. Cao, P. Zhang, J. Sun, H. Zhu, J. Wang, X. Gao, N. Gao, H. Chang, Y. Sheng, H. Zhang, Z. Wang, Slow positron annihilation studies on helium irradiated tungsten, Nucl. Instrum. Methods Phys. Res., Sect. B 406 (2017) 578–584, https://doi.org/10.1016/j.nimb.2017.03.127.
[48] T. Zhu, S. Jin, P. Zhang, L. Song, X. Lian, P. Fan, Q. Zhang, D. Yuan, H. Wu, R. Yu, X. Cao, Q. Xu, B. Wang, Characterization of helium-vacancy complexes in He-ions implanted Fe9Cr by using positron annihilation spectroscopy, J. Nucl. Mater. 505 (2018) 69–72, https://doi.org/10.1016/j.jnucmat.2018.03.048.
[49] S.M. He, N.H. van Dijk, M. Paladugu, H. Schut, J. Kohlbrecher, F.D. Tichelaar, S. van der Zwaag, In situ determination of aging precipitation in deformed Fe-Cu and Fe-Cu-B-N alloys by time-resolved small-angle neutron scattering, Phys. Rev. B 82 (2010), https://doi.org/10.1103/PhysRevB.82.174111.
[50] C.D. Versteylen, N.H. van Dijk, M.H.F. Sluiter, First-principles analysis of solute diffusion in dilute bcc Fe-X alloys, Phys. Rev. B 96 (2017), https://doi.org/10.1103/PhysRevB.96.094105.
[51] C.S. Becquart, C. Domain, Ab initio contribution to the study of complexes formed during dilute FeCu alloys radiation, Nucl. Instrum. Methods Phys. Res., Sect. B 202 (2003) 44–50, https://doi.org/10.1016/s0168-583x(02)01828-1.